Raman study of thin films from amorphous-to-microcrystalline silicon prepared by hot-wire chemical vapor deposition

Daxing Han, J.D. Lorentzen, J.R. Weinberg-Wolf, and L.E. McNeil, Department of Physics & Astronomy, University of North Carolina at Chapel Hill, Chapel Hill, NC 27599-3255, USA

Qi Wang
National Renewable Energy Laboratory, Golden, CO 80401, USA

Abstract

The structure changes of thin films from amorphous (a) to microcrystalline (μc) silicon are studied by Raman scattering in terms of three deposition parameters: silane flow rate, hydrogen flow rate, and total gas pressure in hot-wire chemical vapor deposition. The Raman TO mode is deconvoluted into two Gaussian functions for the a-Si:H and intermediate components and one Lorenzian function for the c-Si component. We found that: (a) in general, the structure change is a function of the ratio of hydrogen to silane gas flows, R, but also depends on the SiH_4 flow rate and total gas pressure; (b) there is a narrow structural transition region in which the short-range order of the a-Si:H network improves, i.e., the bond-angle variation of the a-Si network decreases from ~10˚ to ~8˚ once the c-Si grains start to grow; and (c) when the films were deposited using a high SiH_4 flow rate of 22 sccm, the narrow TO mode with low peak frequency could be related to the column-like structures.

PACS number: 73.61.Jc; 78.20.Jq; 78.55.-m.

I. INTRODUCTION

Transition films from amorphous hydrogenated silicon (a-Si:H) to microcrystalline (μc) silicon have attracted a great deal of attention because the most stable, high-performance a-Si:H solar cells ever achieved were prepared at just before the onset of microcrystallinity [1]. In addition, increasing crystalline silicon (c-Si) volume fraction and grain size and reducing defects are important issues for thin c-Si films and their device applications [2,3]. Generally, the μc-Si:H structure contains an a-Si:H matrix, c-Si grains, grain boundaries (g.b.), and microvoids [4,5]. Such materials exhibit a variety of microstructures and properties that depend on preparation conditions. Compared to other deposition techniques, such as high-H-dilution of plasma-enhanced (PE) CVD and very-high-frequency (VHF) PE-CVD [6-8], the advantage of using the hot-wire (HW) CVD technique is its high deposition rate [4].

Raman spectroscopy is a sensitive tool that provides valuable structural information about a-Si-based materials [9]. In a-Si, all phonon modes of the transverse acoustic (TA), longitudinal acoustic (LA), longitudinal optical (LO), and transverse optical (TO) modes are Raman active. Thus, Raman spectra from a-Si at room temperature yield a reasonable spectral comparison with phonon density of states that are modified substantially by small changes in short-range order (SRO) [8-10]. Theoretical calculations found that the full width of half maximum (FWHM), Γ, the peak frequency of the TO phonon mode (ω_{TO}), and the relative intensity of the TA mode, TA/TO, are sensitive to bond-angle variation (ΔΘ) in an a-Si network [8-10]. Beeman et al. [10] found a linear relationship between the width of the TO mode and the spread in the mean bond angle ΔΘ in an a-Si network as

$$\Gamma = 15 + 6\Delta\Theta. \quad (1)$$

More recent calculations using 1000-atom configurations [11] showed a similar relation of $\Gamma=18.4 + 6.6\Delta\Theta$ and a shift of the TO mode frequency toward higher frequency as $\Delta\Theta$ decreases following

$$\omega_{TO} = -2.5\ \Delta\Theta + 505.5 \qquad (2)$$

for HV-polarized light. The authors [11] further found that the TA/TO intensity ratio decreases linearly with decreasing $\Delta\Theta$. For device-quality a-Si:H, the TO mode centered at 480 cm^{-1} with FWHM ≈ 70 cm^{-1}. According to equation (1), the spread in mean bond angle $\Delta\Theta$ is ≤10°. In c-Si, on the other hand, the Raman spectrum consists of a single sharp TO mode with FWHM of 4 cm^{-1} at a frequency of 520 cm^{-1}. All other modes are not Raman active, because of the symmetry in the fcc lattice. However, when the c-Si grain size is as small as a few nm, the momentum conservation will be relaxed and Raman active modes will not be limited to the center of the Brillouin zone. Thus, the frequency could shift from 520 cm^{-1} to ≈512 cm^{-1} with decreasing grain size from ≥10 to ≈3 nm [12-14]. Below 3 nm, a crystalline-to-amorphous transition occurs [14]. In addition to the a-Si and c-Si phonon modes, the Raman TO mode from μc-Si films contains a third intermediate peak centered around 500 ± 10 cm^{-1}, which could be attributed to the contribution of grain boundaries [4,12] or other structures [6]. With hydrogen dilution, Tsu et al. [6] found chainlike objects in PE-CVD films using high-resolution transmission electronic microscopy (TEM), which they claim is evidence for intermediate ordering in H-diluted films. They found that the a-Si TO band centered at 490 cm^{-1} (37 ± 3 cm^{-1} full width) instead of 480 cm^{-1}.

To determine the c-Si volume fraction from the Raman TO mode, one must take into account the differences between a-Si and c-Si with respect to scattering cross sections and optical absorption coefficients. Bustarret et al. [15] found that the ratio of the cross section for the amorphous-to-crystalline phase for grain size > 3 nm at the excitation wavelength 514.5 nm can be written as

$$y(L) = 0.1 + \exp[-(L/250)]. \quad (3)$$

It is expected that y(L) will be 2.4 times smaller at 632.8-nm excitation. Based on the above argument, we deduced the crystalline volume fraction, X_c, from the Raman TO mode using

$$X_c = (I_c + I_{gb})/[I_c + I_{gb} + y(L)I_a], \quad (4)$$

where $I_c + I_{gb}$ and I_a are integrated intensities of the c-Si, intermediate, and a-Si peaks, respectively; y(L) decreases from 1 to 0.4 when the grain size L grows from 3 nm to 30 nm. We found that when using 514.5-nm laser front excitation, X_c can be deduced in such a way to be consistent with the results from x-ray diffraction (XRD) for HW-CVD transition films [4,16].

In previous works [4,16], we reported Raman, XDR, FTIR, photoluminescence, and optical absorption results for HW-CVD films with either varied hydrogen-to-silane ratio, R, with fixed silane flow rate or varied substrate temperature, T_S, at fixed R = 3. We observed a blue shift of the a-Si:H PL peak frequency, which was due to narrowing of the band tail states by hydrogen dilution and a low-energy PL band in the μc-Si films. The low-energy PL band originates from the c-Si g.b. regions, and thus, we have attributed the intermediate component of the Raman TO

mode to the g.b. regions [4,16]. The previous Raman results showed a threshold of $R \approx 2$ at $T_S = 240^{\circ}$-250°C and $T_S \approx 200^{\circ}$C at $R = 3$ for the structural transition from a- to μc-Si:H. Both the threshold growth conditions of crystallinity and the crystalline silicon volume fraction deduced from the Raman TO modes are consistent with the results from X-ray diffraction [4,16]. In this work, we have extended our deposition parameter range to include not only the H-dilution ratio R, but also the effect of silane flow rate and total gas pressure. For example, at a fixed R, the individual SiH_4 and H_2 flow rates can be changed such that one condition has a higher silane flow rate than the other. The films deposited at the same R were not the same and depended on the actual gas flow rates. This systematic study of the correlation between material structure and deposition conditions can help us understand the growth mechanism and adjust the growth conditions of μc-Si:H films.

II. SAMPLE AND EXPERIMENTAL

We deposited 125 intrinsic Si films by HW-CVD on Corning 1737 25 × 25 mm^2 glass using the combinatorial deposition method [17]. All of the films were grown at the same substrate temperature, $T_S = 240^{o}$C. There were four groups with various silane flow rates of 3, 8, 16, and 22 sccm, respectively. The hydrogen flow rate for each group was varied from 0 to 216 sccm. The total gas pressure was controlled by adjusting the throttling valve position (TVP) at 45%, 50%, 60%, 70%, and 80%. The higher percentage leads to lower pressure. The total pressure of the deposition chamber as a function of TVP and H_2 flow rate is listed in Tables I, II, II, and IV for SiH4 = 3, 8, 16, and 22 sccm, respectively. For the films with a low silane flow rate of 3 sccm, the thickness was controlled in the range of 1500-2000 Å, and the growth rate was in the range of 1-3 Å/s; for the films with silane flow rates of 8 and 16 sccm, the thickness was

controlled in the range of 5000-6000 Å, and the growth rate was in the range of 5-13 Å/s; for the films with a silane flow rate of 22 sccm, the thickness was controlled in the range of 0.9-1.1 μm, and the growth rate was in the range of 8-21 Å/s. Two films were made as thin as the penetration depth of the 514.5-nm laser, 60-70 nm, and these were used for calibrating the Raman spectra from back excitation.

Raman spectra were measured using an XY triple spectrograph equipped with a LN_2-cooled CCD detector. The data were taken at room temperature using the 514.5-nm line of an argon-ion laser. The spectral resolution was approximately 0.5 cm^{-1} in a frequency range of 100 to 1000 cm^{-1}. The frequency of the Raman lines were calibrated using the TO mode of a (111) c-Si wafer at 520 cm^{-1}. The power of the laser was kept below the level that would thermally induce crystallization. The penetration depth of the 514.5-nm light is ~60 nm for a-Si:H and is larger for μc-Si:H. Since the Raman spectra reveal the structure of the thin layer, measurements were also done from back-excitation for most samples. To depress the scattering light from the substrate, the light spot was focused on the film using a microscope. The Raman TO mode for all films was deconvoluted into two Gaussian functions and one narrow Lorenzian function to represent the three components of a-Si, intermediate, and c-Si peaks. The c-Si grain size ranged from 7 to 30 nm, which was obtained from XRD [4]; the crystalline volume fraction, X_c, was deduced using equations (3) and (4) with $0.4 < y(L) < 0.85$.

III. RESULTS AND DISCUSSION

In general, the structure change is a function of the ratio of hydrogen-to-silane flows, R [4,16]. Fig. 1(a-p) shows the crystalline silicon volume fraction, X_c, as a function of R for four groups of films at SiH_4 flow rates of 3, 8, 16, and 22 sccm and with the total gas pressure varied

with the throttling valve position (TVP) of 45%, 50%, 60%, 70%, and 80%. The solid and dotted lines indicate the X_c obtained from the top and bottom layer, respectively. The X_c is found from zero to >90% (including $X_{g.b.}$ from zero to ~30%) in the top layers. In agreement with the previous works [4,16], there is a threshold R for the structural transition from a- to μc-Si:H. The common features of the curves in Fig.1(a-p) are: (a) Narrow structure transition region ($\Delta R \sim 1$) from $X_c = 0$ to $\geq 50\%$. We will analyze this transition region in detail shortly. (b) The threshold R of crystallinity increases with increasing SiH_4 flow rates. For instance, the threshold is $R \leq 2$ for low SiH_4 flow rates of 3 and 8 sccm, as shown in Figs. 1(a-g), but no crystallinity has yet occurred at R=2 for high SiH_4 flow rates of 16 and 22 sccm, as shown in Figs. 1(i-p). And (c) the X_c changes with the total pressure in the chamber in the following way: the films easily become μc-Si at the higher pressure (lower TVP) and lower silane flow rates of 3 and 8 sccm, as seen by comparing Figs. 1(a) to 1(d) and 1(e) to 1(h); whereas, at high silane flow rates of 16 and 22 sccm, a lower pressure (higher TVP) yields a higher X_c in the film, as seen by comparing Figs. 1(i) to 1(j) or 1(m) to 1(n). These surprising results suggest that there is a "growth zone" for the crystallite, and it is our intention to study many deposition parameters, and not just R, to examine this further. We explain the (b) and (c) results above by qualitatively using the silane-depletion model. At low flow rate and low pressure, the SiH_4 is almost depleted; but at high flow rate and high pressure, the SiH_4 is partially depleted. The higher degree of SiH_4 depletion, the more crystallinity in the films.

We used back excitation to study the early growth of the film. At the early stage of the growth, X_c is much lower than in the late growth of the films, as shown by the dotted lines in Fig 1. Whereas, in Fig. 1(d) for the film with R = 72 and SiH_4 = 3 sccm, we observe roughly the same X_c value. This is because the film thickness of 70 nm is close to the penetration depth of

the 514.5-nm laser. For such a thin sample, the Raman spectral line shape from the back excitation was almost identical to that from the front excitation. Indeed, the width of the a-Si TO mode was broader (80 cm^{-1}) and the X_c was lower (57 %) for the back excitation compared to FWMH = 67 cm^{-1} and X_c = 63% for the front excitation due to uniformity of both the absorption coefficient and the structure along the vertical direction. For all of the films in this study, the FWMHs of the a-Si network from the bottom layers are in the range of 75-83 cm^{-1}. These values are always broader than the 67-80 cm^{-1} for the top layers. This implies that the a-Si:H network near the glass substrate is less ordered compared to the top surface layer.

Figs. 2(a) and 2(b) show the Raman spectra and their fitting functions for the films with SiH_4 flow of 3 sccm, TVP=45%, and R=1 and 2, respectively. The fittings for the TA mode peaked at 145 cm^{-1} and the LA mode peaked at 330 cm^{-1}, which are also shown. The signal between the TO and LA modes is attributed to the LO mode. Comparing Fig. 2(a) and 2(b), one can see that the intensity ratio of TA/TO decreased as the film was more crystallized. This agrees qualitatively with the theoretical calculations [11]. More importantly, we obtain the structure information from the TO mode according to equations (1) and (2). Figs. 2(c) and 2(d) show the enlarged TO mode fittings between 450 to 550 cm^{-1} for the same samples in Figs. 2(a) and 2(b). The band width of the TO mode, FWHM, and their peak frequency, ω_{TO}, as a function of H-dilution ratio are plotted in Figs. 3(a) and 3(b) for all the films in this study. Generally, the FWHM decreases and the ω_{TO} increases in the narrow structural transition region and then reaches a saturation value. Notice that the films with high SiH_4 flow rate of 22 sccm (the big crosses) show the narrowest FWHM and lowest ω_{TO}. It is perhaps related to column-like structures [18]. The changes can be seen more clearly for the low growth rate films with SiH_4 flow rate of 3 sccm, which are represented by solid dots in both Fig. 3(a) and 3(b).

The improvement of SRO of the a-Si:H network in the a-to-μc-Si transition region is clearly shown in both the changes of FWHM and ω_{TO}. In Fig. 3(a), the FWHM decreases from 80 to 67 cm^{-1} when $0 \leq R \leq 3$, and then remains at 67 cm^{-1} when $R > 3$. This indicates that the spread in mean bond angle $\Delta\Theta$ decreased from 10.8° to 8.6° according to equation (1). The corresponding frequency shift ω_{TO} for the same films in Fig. 3(b) is from 475 cm^{-1} to 480 cm^{-1}, which indicates that the $\Delta\Theta$ decreased from 12.2° to 10.2° according to Eq. (2). The absolute values of $\Delta\Theta$ are relatively large from the calculation [11], but the 2° improvement of the bond angle spread is consistent with the results from the decrease of the band width [10]. The improvement of SRO of the a-Si network by increasing H-dilution is consistent with the observations of narrowing of the valence band tail in our previous work [4,19]. For most of the high-SiH_4-flow-rate films, indicated by the open circles and big crosses, the FWHM = 67 cm^{-1} and does not change with R, but the ω_{TO} spreads from 475 to 480 cm^{-1} at $0<R<3$. Whereas, the FWHM is as narrow as 58.5 cm^{-1} and the peak frequency as low as 472 cm^{-1} for the films deposited with the highest growth rate of ~20 Å/s (represented by the big crosses). The frequencies of the c-Si and g.b. peaks for those films are also low (see Figs. 4 and 5). Since a column-type growth occurs in such conditions [18], it implies that both the ω_{TO} and the FWHM are sensitive to the column structures. To our knowledge, there are no calculations of how the phonon density of states changes with such structures.

For the c-Si component, we generally found that the width of the c-Si TO mode for the μc-Si:H films is broader than that for the c-Si wafer, i.e., 8-10 cm^{-1} compared to 4 cm^{-1}. There were two exceptions for films with SiH_4=3 sccm with TPV=70% and R=1.2 and 3. The reason is unclear why the FWHM was as narrow as 4 cm^{-1} for those two films. However, the peak frequency of the c-Si TO mode, $\omega_{c\text{-}Si}$, changes when R increases. For the films with SiH_4 flow

rate of 3 and 8 sccm, we found a blue shift from 516 to 520 cm^{-1} in the transition region, as shown in Fig. 4. This indicates that of the crystallite size has increased from ~7 nm to ≥ 10 nm [12-14]. For the films with high SiH_4 flow rate of 22 sccm, the big crosses indicate that the $\omega_{c\text{-}Si}$ blue shift occurs from 513 to 518 cm^{-1}. Again, the relatively low frequency of the c-Si TO mode could be due to the column-like structures.

Finally, for all the μc-Si:H films, the Raman TO mode always contains an intermediate component in addition to the a-Si and c-Si components. The intermediate component was fitted well using a Gaussian function with FWHM of 33 cm^{-1} for all the μc-Si:H films. The peak frequency of the intermediate component, $\omega_{g.b}$, as a function of R is plotted in Fig. 5. One finds that the value spreads from 500 to 510 cm^{-1}. For the low-growth-rate films, there is a blue shift of the $\omega_{g.b}$ from 500 to 507 cm^{-1} in the transition region and then spreads between 505 to 507 cm^{-1} when R >3. Regardless of whether the intermediate component originates from the grain boundaries, small size (<3 nm) crystallites [4,12], or median-range ordered objects [5], the blue shift of the $\omega_{g.b}$ can be attributed to the growth of the c-Si grain size. One may argue that Raman modes reflect SRO, and the phonon density of states is sensitive to the local bond angles [9-11]. However, the scattering intensity is related to a coupling-parameter-weighted phonon density of states. Small differences between peak positions could be attributed to changes in median- or long-range interactions that are consequences of the coupling parameter. We could not clarify the origin of this intermediate component in this work. Whatever the origin is, one commonly takes the third component into account as part of the c-Si volume fraction, as seen in equation (4).

As shown above, the peak frequencies of all the three components of the TO modes show blue shift with increasing of H-dilution in the structural transition region. The compressive stress

could be higher in films with higher hydrogen dilution ratios (the film easily peels off from the substrate), and the blue shift of the phonon bands could be partially related to an increase of the film stress.

VI. SUMMARY

Raman scattering studies were carried out on the transition films from amorphous-to-microcrystalline silicon prepared by HW-CVD with varied silane and hydrogen flow rates and the T-valve position. The measurements were done for both front and back excitation. The TO mode was deconvoluted into a broad Gaussian function for the a-Si:H and a narrow Lorenzian function for the c-Si; a Gaussian function peaked at between 500 to 510 cm^{-1} with FWHM of 33 cm^{-1} for the intermediate component. We believe that origin of the intermediate component is the grain boundaries and the small-size (< 3 nm) crystallites [4,12], and attribute it into the total c-Si volume fraction. The c-Si volume fraction depends not only on the H-dilution ratio, $R= H_2/SiH_4$, and the film thickness, but also on the SiH_4 flow rate and total gas pressure, which can be explained using the silane-depletion model. The detailed calculation of gas depletion will be reported in a future work.

The most interesting finding is a narrow structural transition region of $\Delta R \sim 1$, in which the short-range order of the a-Si:H network is improved: the width of the TO mode decreased from 80 to 67 cm^{-1} and the peak frequency, ω_{TO}, blue shift from 475 to 480 cm^{-1}. These indicate that the bond-angle variation, $\Delta\Theta$, of the a-Si network decrease from ~10˚ to ~8˚ when the crystallites start to grow. Furthermore, the crystallite grain size increases from ~7 nm to ≥ 10 nm in the transition region, evident by a blue shift of the c-Si mode, $\omega_{c\text{-}Si}$, from 516 to 520 cm^{-1} [12-14]. When R continually increases beyond the transition region, the SRO of the a-Si:H

network, the c-Si volume fraction, and the c-Si peak frequency, somewhat, are saturated. However, the structure would be continually modified at higher hydrogen dilution ratio. Other techniques such as TEM will assist in clarifying the further structural changes.

Finally, when the films were deposited with high growth rate ~20 Å/s using high SiH_4 flow rate, the FWHM of the TO mode for a-Si network can be as narrow as 58.5 cm^{-1} and the peak frequency as low as 472 cm^{-1}. A column-type growth occurs in such conditions [18], which implies that both the ω_{TO} and the FWHM are sensitive to the column structures. Calculations are needed to find how the phonon density of states changes with such structures.

AKNOWLEDGEMENT

This work is supported by NREL Subcontract No. ADJ-1-30630-09 at the Univ. of North Carolina and by the U.S. DOE under Contract No. DE-AC36-99GO10337.

References

1. S. Guha, J. Yang, D.L. Williamson, Y. Lubianiker, J.D. Cohen, and A.H. Mahan, Appl. Phys. Lett. **74**, 1860 (1999).
2. J.K. Kim, J.Y. Lee, and K.S. Nam, J. Appl. Phys. **77**, 95 (1995).
3. J. Meier, P. Torres, R. Platz, S. Dubail, U. Kroll, J.A. Anna Selvan, N. Pellaton Vaucher, Ch. Hof, D. Fischer, H. Keppner, A. Shah, K.-D. Ufert, P. Giannoules, and J. Koehler, "Amorphous Silicon Technology" edited by M. Hack, E.A. Schiff, S. Wagner, R. Schropp, and A. Matsuda, MRS Symp. Proc Vol **420**, 3 (1996).
4. Guozhen Yue, J. D. Lorentzen, Jing Lin, Qi Wang, and Daxing Han, Appl. Phys. Lett. **75**, 492 (1999).

5. Guozhen Yue, Daxing Han, D.L. Williamson, Jeffrey Yang, Kenneth Lord, and Subhendu Guha, Appl. Phys. Lett. **77**, 3185-3187 (2000).
6. D. V. Tsu, B. S. Chao, S. R. Ovshinsky, S.J. Jones, J. Yang and S. Guha, Phys. Rev. B **63**, (2001) 125338.
7. M. Luysberg, P. Hapke, R. Carius, and F. Finger, Phil. Mag. A **75**, 31 (1997).
8. L. Houben, M. Luysberg, P. Hapke, R. Carius, F. Finger, and H. Wagner, Phil. Mag. A **77**, 1447 (1998).
9. J.S. Lannin, in Semiconductors and Semimetals, Vol 21, part B, chapter 6, edited by J. L. Pankove, (Academic Press, Inc., London, 1984).
10. D. Beeman, R. Tsu, and M.F. Thorpe, Phys. Rev. B **32**, 874 (1985).
11. R. L. C. Vink, G. T. Barkema, and W.F. van der Weg, Phys. Rev. B **63**, 115210 (2001).
12. S. Veprek, F. A. Sarott, and Z. Iqbal, Phys. Rev. B **36**, 3344 (1987).
13. Yuliang He, Chenzhong Yin, Guangxu Cheng, Luchun Wang, Xiangna Liu, and G.Y. Hu, J. Appl. Phys, **75**, 797 (1994).
14. S. Veprek, Z. Iqbal, and F. A. Sarott, Philos. Mag. B **45**, 137 (1982).
15. E. Bustarret, M.A. Hachicha, and M. Brunel, Appl. Phys. Lett. 52, 1675 (1988).
16. Daxing Han, Keda Wang, Jessica M. Owens, Lynn Gedvilas, Brent Nelson, Hitoe Habuchi, and Masako Tanaka, J. Appl. Phys (in press, April 1, 2003).
17. Qi Wang, Guozhen Yue, Jing Lin, and Daxing Han, Solid State Commun. **113**, 175 (2000).
18. A. H. Mahan, Y. Xu, D. L. Williamson, W. Beyer, J. D. Perkins, M. Vanecek, L. M. Gedvilas, and B. P. Nelson, J. Appl. Phys. **90**, 5038 (2001).
19. Daxing Han, Keda Wang, and Liyou Yang, J. Appl. Phys. **80**, 2475-2482 (1996).

Figure captions

Fig. 1. Crystalline volume fraction as a function of H-dilution ratio at SiH_4 flow rates of 3, 8, 16 and 22 sccm. The solid and dotted lines indicate the X_c was obtained from the top or bottom layer of ≥ 60 nm, respectively.

Fig. 2. Raman shift and their fitting functions from the films with SiH_4 flow of 3 sccm, TVP=45%, and (a) R=1 with fitting functions of c1=330*exp(-((c0-475)/40)^2), c2=11800/((c0-518)^2+5.5^2), c3=140*exp(-((c0-500)/20)^2), c4=80*exp(-((c0-145)/50)^2), and c5=50*exp(-((c0-330)/70)^2); (b) R=2 with fitting functions of c1=480*exp(-((c0-480)/40)^2), c2=30000/((c0-518.5)^2+4.5^2), c3=350*exp(-((c0-507)/20)^2), c4=75*exp(-((c0-145)/50)^2), and c5=70*exp(-((c0-330)/70)^2); and the enlarged TO mode between 450 cm^{-1} to 550 cm^{-1} with their fitting functions of c1+c2+c3 in (c) and (d).

Figs. 3.(a) The band width and (b) the peak frequency of the a-Si TO mode as function of hydrogen dilution ratio. The solid dots, dashes, open circles, and crosses represent the films with SiH_4 flow rate of 3, 8, 16, and 22 sccm, respectively. There are two regimes separated at R≈3: the fast changing regime when R <3 and the saturated regime when R>3.

Fig. 4. The peak frequency of c-Si as a function of R.

Fig. 5. The intermediate component peak frequency of the TO mode as a function of R.

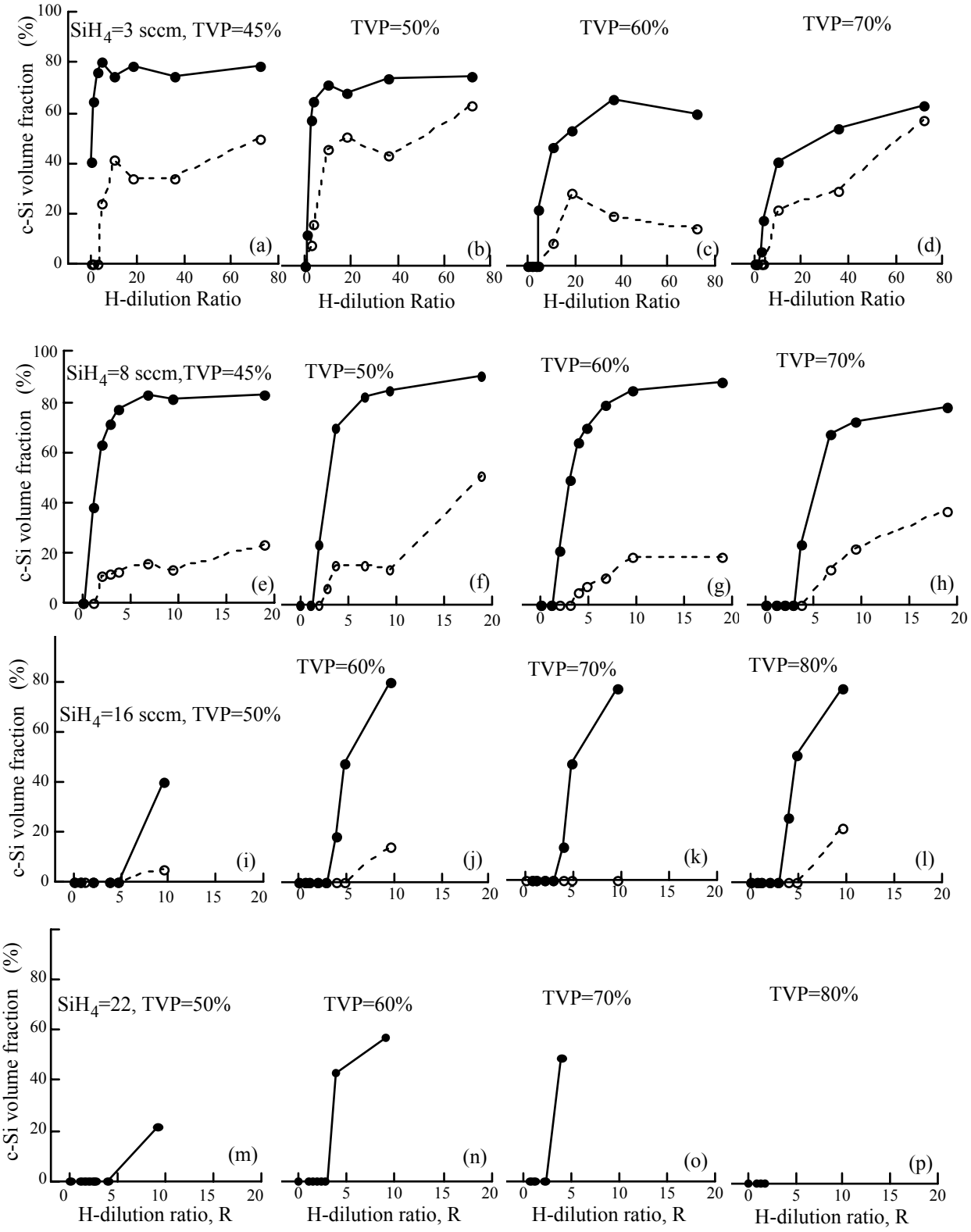

Fig. 1/D. Han et al

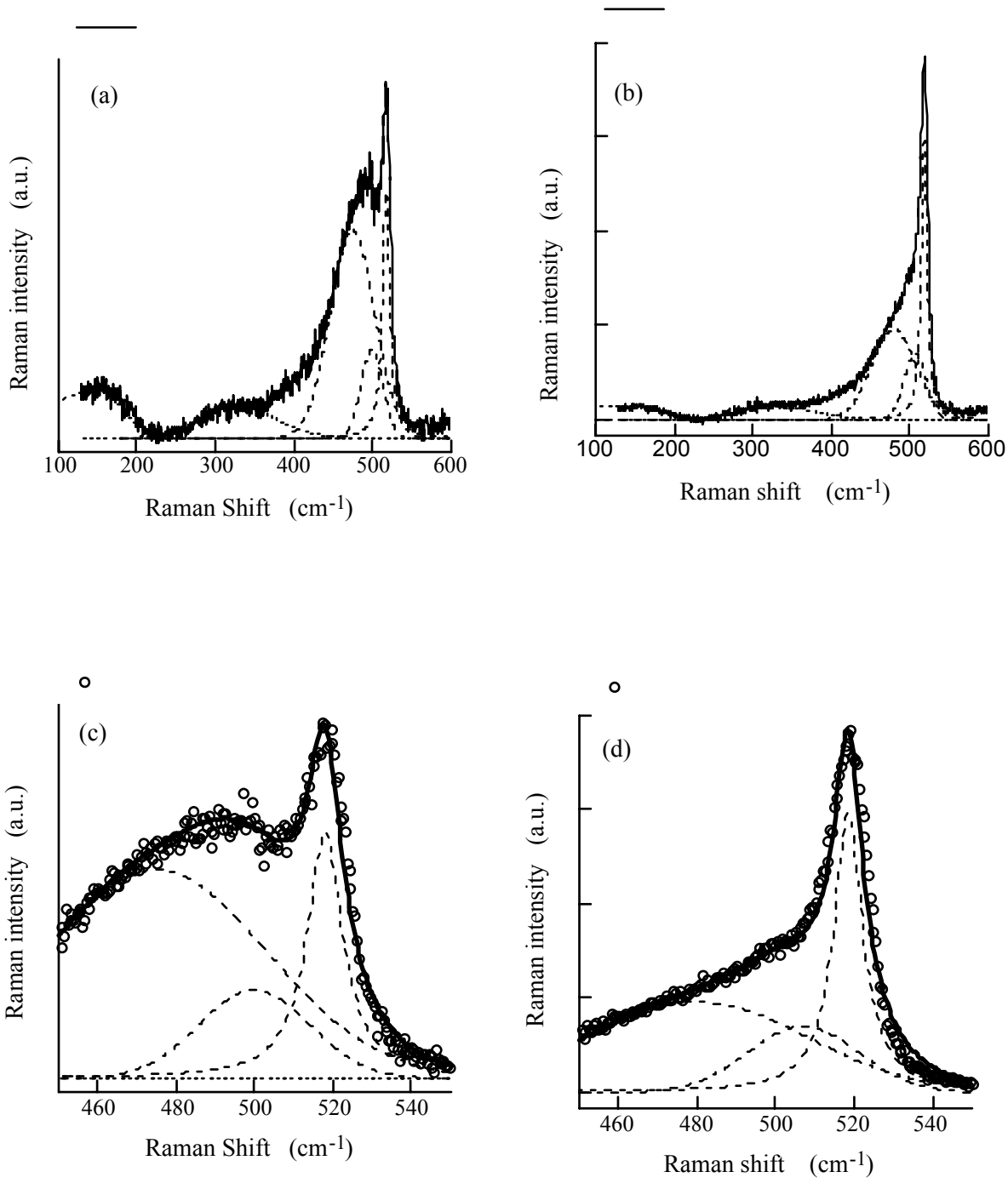

Figs. 2(a), 2(b), 2(c) and 2(d)/D. Han et al

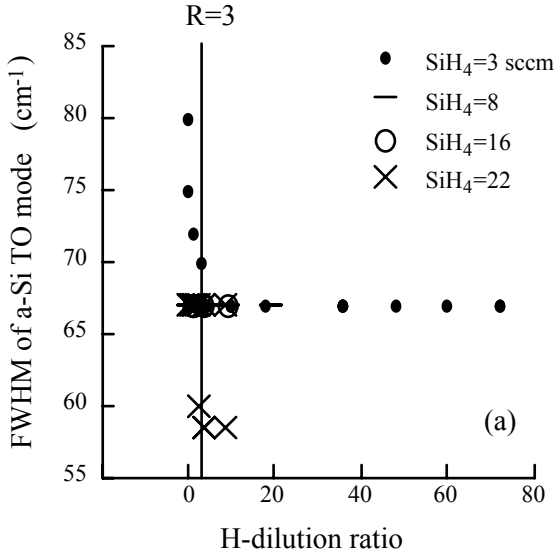

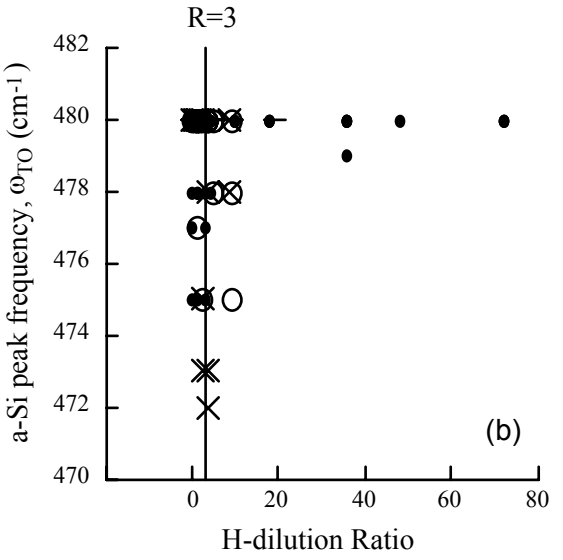

Figs. 3(a) and 3(b)/D. Han et al

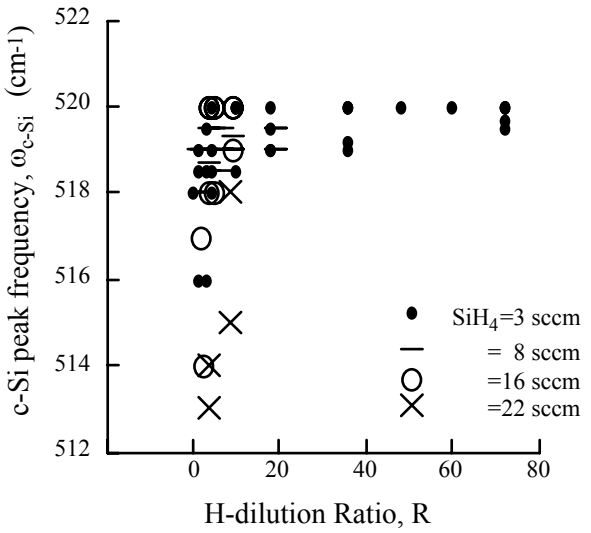

Fig. 4/D.Han et al

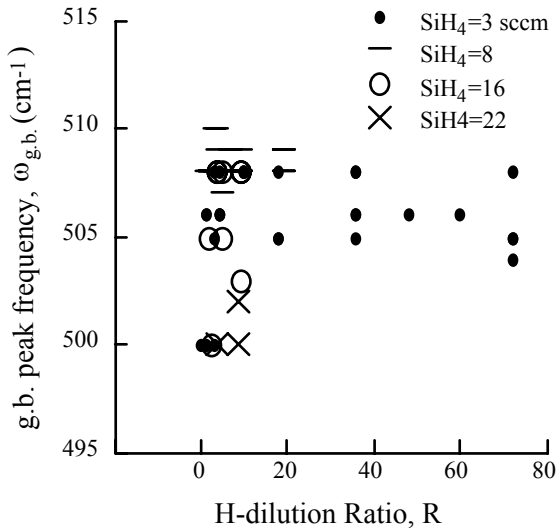

Fig. 5/D.Han et al

Table I. The total gas pressure as a function of TVP at SiH_4 = 3 sccm

	TVP (%)			
	45	50	60	70
H_2 (sccm)	Total gas pressure (mTorr)			
0	12	7	4	3
3.6	13	9	5	4
9	20	12	7	5
12.6	25	14	8	6
30.6	47	30	14	26
54	75	47	21	35
108	139	88	37	45
216	267	172	77	56

Table II. The total gas pressure as a function of TVP at SiH_4 = 8 sccm

	TVP (%)			
	45	50	60	70
H_2 (sccm)	Total gas pressure (mTorr)			
0	24	14	10	4
9	36	20	14	6
16.2	45	25	18	8
23.4	54	30	21	10
30.6	64	36	25	11
54	95	53	36	17
75.6	120	69	46	21
151.2	210	121	84	40

Table III. The total gas pressure as a function of TVP at SiH_4 = 16 sccm

	TVP (%)			
	50	60	70	80
H_2 (sccm)	Total gas pressure (mTorr)			
0	25	12	7	6
9	30	15	9	7
16.2	35	18	11	9
30.6	44	22	13	11
45	49	27	15	13
61.2	59	31	18	16
75.6	66	36	21	18
153	109	60	38	33

Table IV. The total gas pressure as a function of TVP at SiH_4 = 22 sccm

	TVP (%)			
	50	60	70	80
H_2 (sccm)	Total gas pressure (mTorr)			
0	33	16	10	8
21.6	45	22	14	11
30.6	50	24	16	12
41.4	57	28	18	14
52.2	61	28	20	17
57.6	65	32	21	18
82.8	79	39	26	22
198	148	76	54	48